GEODINAMICA ACTA
2018, VOL. 30, NO. 1, 249–264
https://doi.org/10.1080/09853111.2018.1494776

Taylor & Francis
Taylor & Francis Group

ARTICLE

OPEN ACCESS Check for updates

Geomorphic evidence for active tectonic deformation in the coastal part of Eastern Black Sea, Eastern Pontides, Turkey

Mustafa Softa [a,b], Tahir Emre [a], Hasan Sözbilir [a], Joel Q. G. Spencer [c] and Mehmet Turan [d]

[a]Department of Geological Engineering, Dokuz Eylül University, Izmir, Turkey; [b]The Graduate School of Natural and Applied Sciences, Dokuz Eylül University, Izmir, Turkey; [c]Department of Geology, Kansas State University, Manhattan, Kansas, USA; [d]Department of Geological Engineering, Karadeniz Technical University, Trabzon, Turkey

ABSTRACT

The Eastern Pontides (EP), which is the under transpressional deformation zone, is an active mountain belt that has been rising rapidly since the Cenozoic era because of the Arabian-Eurasian convergence. Morphometric studies have been performed to investigate the tectonic activity of this region and better understand the characteristics of the faults geomorphologically; the faults control the mountain fronts in the drainage basin of the EP. The results show the Hypsometric Curve (HC)-Hypsometric Integral (0.37-HI-0.67), Basin-Shaped Analysis (1.2-B_s-7), Valley-Floor-Width to Height-Ratio (0.4-V_f-1.2) and Asymmetry Factor (35-AF-81) applied to 46 drainage basins together with 9 tectonically controlled geomorphic indices (1.2-S_{mf}-1.5) and a Stream Length Gradient (30-S_L-120) indicate that the EP is tectonically active, and when the areas are evaluated according to S_{mf} and V_f analyses, the tectonic level is relatively high. According to our conceptual model for the uplifting of the EP, with respect to field studies and morphometric analysis, (i) the EP is the active deformation zone and has a "push-up" geometry in conjunction with the North Anatolian Fault; (ii) the EP is progressively uplifting at a rate of more than 0.5 mm/yr in along with the thrust faults of the Black Sea Fault (BSF) and Borjomi-Kazbegi Fault (BKF).

ARTICLE HISTORY
Received 13 March 2018
Accepted 27 June 2018

KEYWORDS
Tectonic geomorphology; Eastern Pontides; mountain fronts; North Anatolian Fault; active tectonic

1. Introduction

Landscape evolution is mostly related between active tectonics and surface processes. These events cause the formation of remarkable geomorphic indicators along the fault-controlled landforms. The most characteristic landforms are seen in orogenic areas, which are tectonically active areas and fault-controlled mountain fronts. Continuously changing landforms by tectonic processes can be overprinted by tectonic structures in a drainage basin. The coastal region of the Eastern Pontides shows geologic and geomorphologic indications suggestive of significant regional tectonic activity since Cenozoic times (Keskin, Pedoja, & Bektaş, 2011; Softa, Spencer, Emre, Sözbilir, & Turan, 2017). The aim of tectonic geomorphology is quantifying the geomorphic response of the landscape to the interaction between active tectonic and geomorphic processes (Mayer, 1986). The quantitative measurement of the landscape is based on the calculation of geomorphic indices using topographic maps and field work (Keller & Pinter, 2002). Morphological analyses offer valuable information to illuminate the tectonic evolution of a region (Keller, 1986; Mayer, 1986). The methods applied to the study of drainage basins are sensitive to active faulting and tectonics, especially uplifting areas. Analyses such as, mountain-front sinuosity, drainage basin shape, stream channel asymmetry, and stream length gradients, are tools for analyzing the tectonically active areas (Bull, 1977; Bull & McFadden, 1977; Gürbüz & Gürer, 2008; Keller, 1986; Keller & Pinter, 2002; Özkaymak, 2015; Özkaymak & Sözbilir, 2012; Ramírez-Herrera, 1998; Silva, Goy, Zazo, & Bardají, 2003; Tepe & Sözbilir, 2017; Troiani, Galve, Piacentini, Della Seta, & Guerrero, 2014; Wells et al., 1988; Yıldırım, 2014).

There are very few morphometric-based uplift rate studies in the Pontides. Most of them focused on absolute dating studies to find uplift rates. According to the OSL ages, the uplift rate was obtained in the Central Pontides, ranging from 0.02 to 0.23 mm/y (Yıldırım et al., 2013). On the other hand, the uplift rate around the Trabzon region was obtained by using ESR dating; macro Gastropod and Bivalvia fossils were taken from the marine terraces in the Eastern Pontides. According to these results, the Trabzon region exhibits uplift rates between 0.06 and 0.17 mm/y (Keskin et al., 2011). However, we have suggested that these rates are very low, and we re-calculated the uplift rate using the OSL age, with these results ranging from 0.59 to 1 mm/y since Cenozoic time (Softa et al., 2017).

In this context, S_{mf} and V_f analyses, as well as other morphometric analyses commonly used in active

CONTACT Mustafa Softa mustafa.softa@deu.edu.tr Department of Geological Engineering, Dokuz Eylül University, Member of Active Fault Research Group, 35390 Izmir, Turkey

© 2018 The Author(s). Published by Informa UK Limited, trading as Taylor & Francis Group.
This is an Open Access article distributed under the terms of the Creative Commons Attribution License (http://creativecommons.org/licenses/by/4.0/), which permits unrestricted use, distribution, and reproduction in any medium, provided the original work is properly cited.

tectonic studies, have been applied in this study. These methods have been used successfully in many countries and prove useful in the investigation of the current the activity of different areas such as in America, Iran, Spain, Italy and Turkey (e.g. Bagha et al., 2014; El Hamdouni, Irigaray, Fernández, Chacón, & Keller, 2008; Pavano, Pazzaglia, & Catalano, 2016; Troiani et al., 2014; Yıldırım, 2014). However, this is the first study to investigate the geomorphology and active tectonics of the Eastern Pontides.

The NAF is one of the most active structures of the region and forms the northern block of the Eastern Pontides, and it corresponds to the northward movement of the Arabian plate (Barka, 1992; Dewey & Şengör, 1979; McKenzie, 1972, 1978), (Figure 1). The present relief of the Eastern Pontides is related to post-collisional scale events. As a result of these events, the presence of normal faults that cutting current sediments and control has caused the mountain front to be determined (e.g. Yılmaz, 2017). This tectonic scenario is the best opportunity to morphologically test the faults that control the mountain front. In this sense, the activities of the faults controlling nine mountain fronts in the northern part of the Eastern Pontides were interpreted as relative. This study is not only the first study to evaluate the control systems of mountain fronts with the elevation model and uplift rate of the region but also the first study to determine the relative activities of the controlling faults of mountainous fronts. At the same time, this study sheds light on the future seismic hazard and risk analysis studies in the Eastern Pontides.

2. Geological setting

The Eastern Pontides, part of the Tethyan Ocean, also known as the East Black Sea mountain belt, forms the middle part of the Alpine Himalayan mountain range and is approximately 1100 km in the east-west vicinity (Figure 1). Although numerous studies have been performed to clarify the geodynamic evolution of the Eastern Pontides, it is still controversial because structural, geochemical, geochronologic data in the region are not reliable. The studies in the region have three views on the subduction polarity of the Eastern Pontides. Adamia, Lordkipanidze, and Zakariadze (1977) and Ustaömer and Robertson (1996) argued that the Eastern Pontides are composed of a Paleozoic plate with a northward subduction until the end of the Eocene. In contrast, Şengör and Yılmaz (1981) argued that the Paleotethys ocean is located

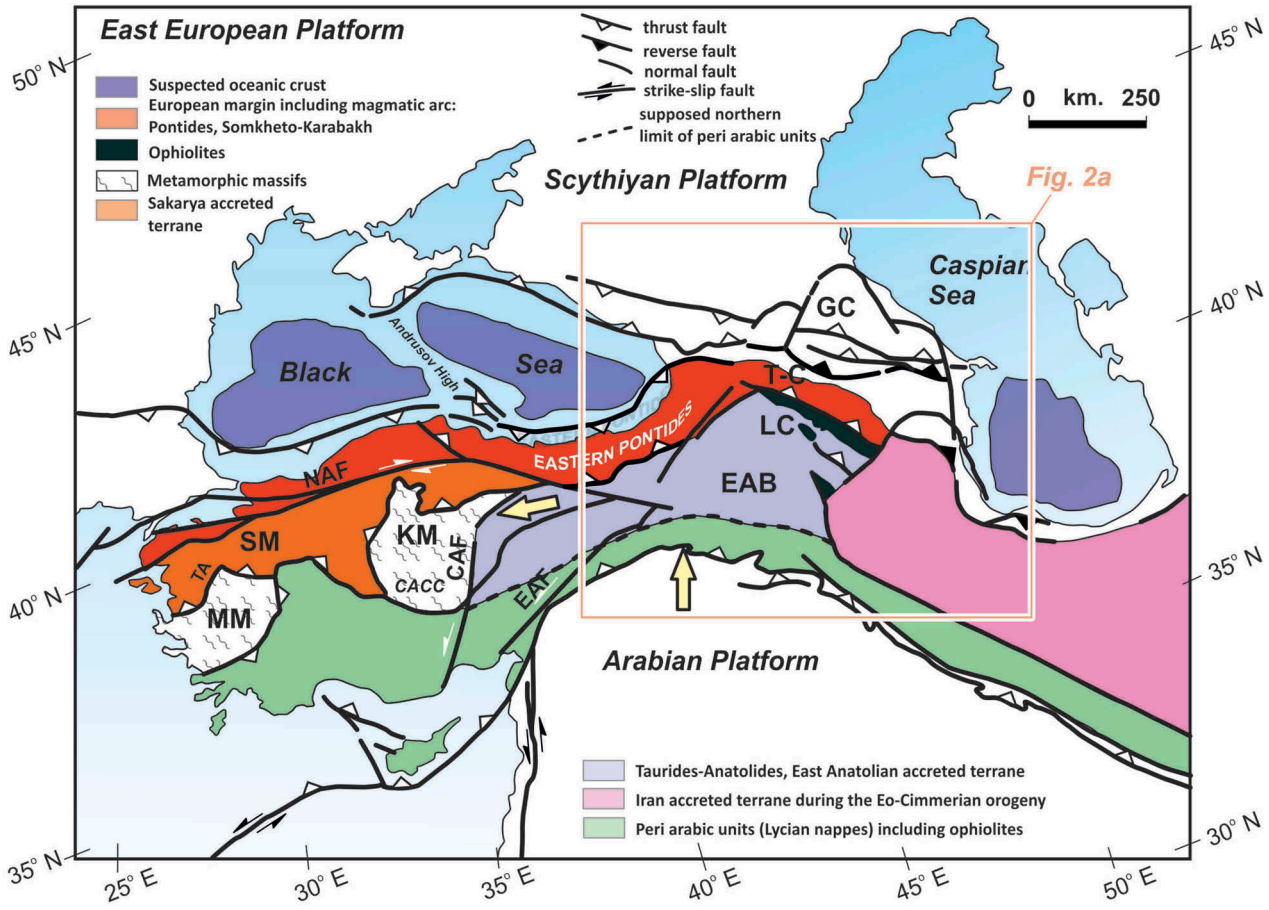


Figure 1. General geological map of the Anatolia – Caucasus region, after Rolland et al. (2016) and Sosson et al. (2010) with modifications. NAF: North Anatolian Fault, CAF: Central Anatolian Fault, EAF: East Anatolian Fault, GC: Greater Caucasus, LC: Lesser Caucasus, T-C: Trans Caucasus, KM: Kirsehir Massif, MM: Menderes Massif, SM: Sakarya Massif, CACC: Central Anatolian Crystalline Complex, EAB: East Anatolian Block.

to the north of the Pontides and that there must be southward subduction from the Paleozoic to the Middle Jurassic and a northward trend toward the Upper Cretaceous to the Eocene. In the third model, Dewey, Pitman, Ryan, and Bonnin (1973); Chorowicz, Dhont, and Adıyaman (1998); Bektaş, Şen, Atıcı, and Köprübası (1999); Eyuboglu et al. (2006); Eyuboglu, Bektaş,, and Pul (2007), Eyuboglu, Santosh, Bektaş, and Ayhan (2011) suggested that an uninterrupted southward subduction polarity lasted from the Paleozoic to the end of Eocene. In this model, the Black Sea was thought to be the remnant of the Tethyan ocean, and the axis zone of ophiolitic rocks were seen as a back-arc basin.

The Eastern Pontides, which is located in the northern block of the NAF, is approximately 500 km long and 200 km wide (Figure 2a). It is divided into 3 main zones and each zone is separated by E-W, NE-SW, and NW-SE trending fault zones with block-faulting (Bektaş & Çapkınoğlu, 1997; Bektaş, Çapkınoğlu, & Akdağ, 2001; Eyuboglu et al., 2006). The northern zone consists mainly of the sediments are magmatic units as volcanic and igneous rocks, including clastic rocks and carbonates from the Paleozoic-Cenozoic. Paleozoic schists and phyllites, which contain moderate alterations, are mapped approximately 20 km to the south of the study area.

Common granitic intrusions date to the Mesozoic and Cenozoic (Güven, 1993), whereas later Pliocene rocks are mostly composed of sandstone, limestone, and marls, were mapped on the mountain fronts and in the immediate vicinity (Figure 3). The youngest unit, the Quaternary alluvium and terraces, is mostly observed on fault-controlled mountain fronts.

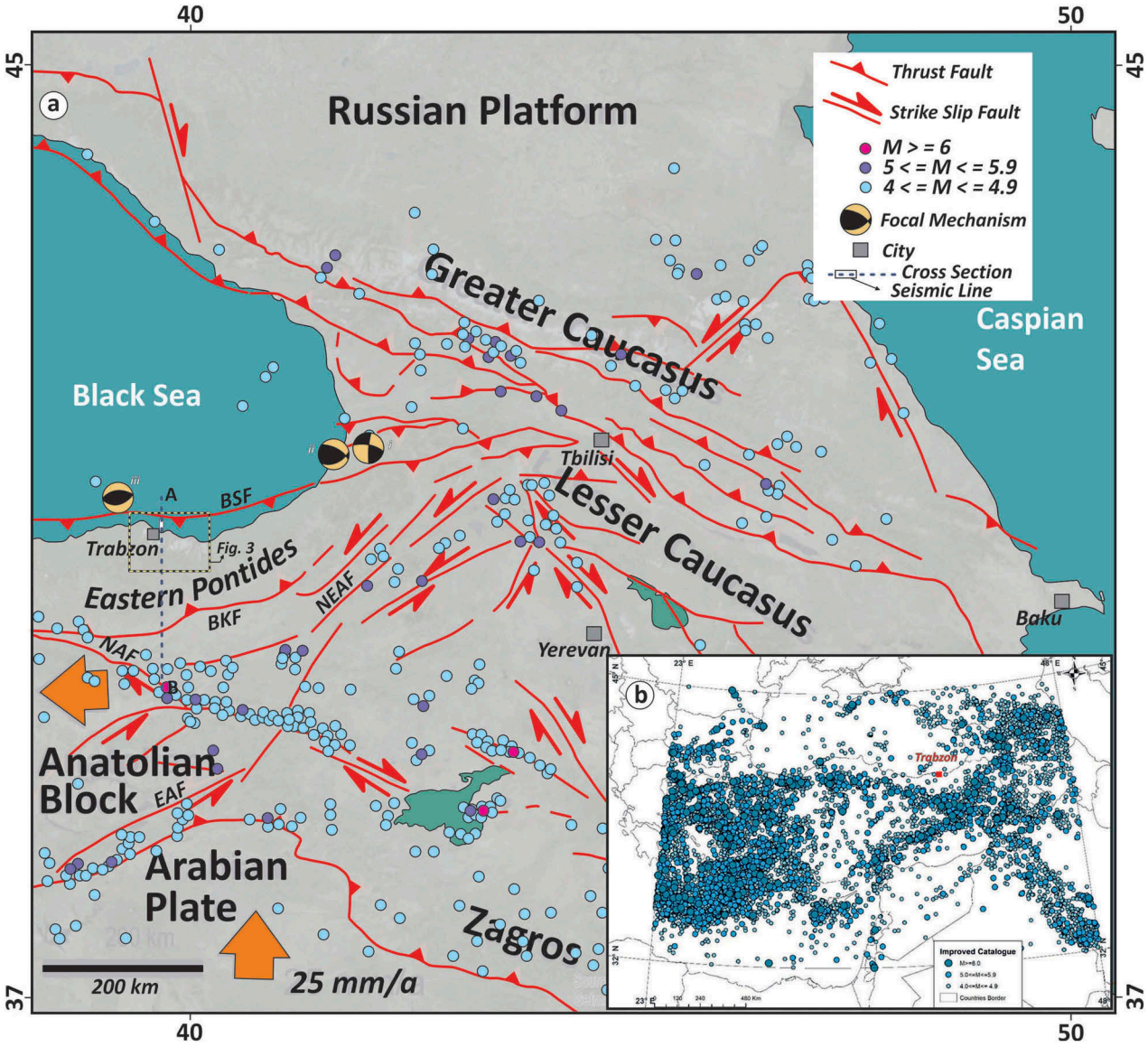


Figure 2. a) Simplified neotectonic map of Eastern Pontides and nearest region (modified from Tsereteli et al., 2016; Avagyan et al., 2010). Earthquake distributions are compiled from the ISC catalogue. NAF: North Anatolian Fault, EAF; East Anatolian Fault, NEAF; Northeast Anatolian Fault, BSF; Borjomi-Kazbegi Fault, BKF; Black sea Fault. b) Inset map showing seismicity of Turkey and its vicinity (Kadirioğlu & Kartal, 2016).

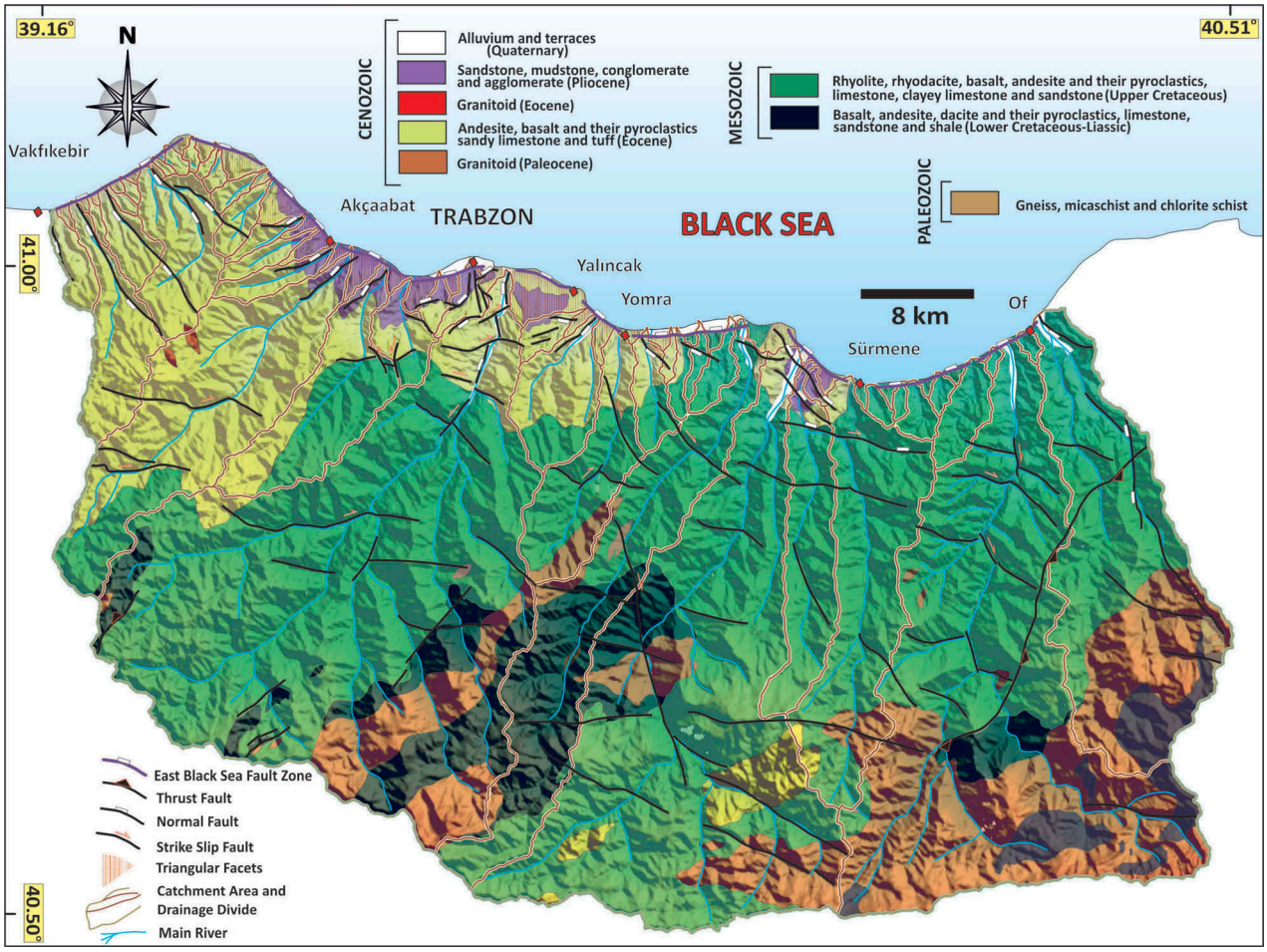


Figure 3. Schematic geological map (modified from Güven, 2003) and its relationships with the catchments showing the main geomorphic indices calculated in this study. Hillshade generated from SRTM (Shuttle Radar Topography Mission) data available at http://earthdata.nasa.gov.

The southern zone is composed of sedimentary, ultramafic, granitic, and metamorphic rocks from the Mesozoic and Eocene. Upper mantle peridotites and Middle-Upper Cretaceous olistrostromal mélange are mostly seen in the axial zone.

3. Seismotectonic setting

The post-Late Orogenic tectonic regime deformation of the Arabian plate, which is the result of N-NW direction movement, shows the movement to the west by moving in an anti-clockwise direction of Anatolia given the current GPS data (Şengör et al., 2008). The relative rates of the Arabian plate moving in the direction of N-NW continue to increase to the west. These rates range from 15–20 mm/y to 30–35 mm/y (Kahle et al., 2000; Reilinger et al., 1997, 2006; Taymaz, Yılmaz, & Dilek, 2007).

The northwards progression of the Arabian plate and resultant compression result in the shortening of Eastern Anatolia, and formation of the right lateral NAF (Figure 2a). The NAF is approximately 1200 km in length and strikes ~ E-W (Fichtner et al., 2013; Şengör, 1979). The fault geometry depicts a convex arc and extends parallel to the Black Sea coasts. Geodetic studies show that the slip velocity of the fault is 24 mm/yr (Reilinger et al., 2006). Insar studies and morphometric studies show that the strain in the region is transferred by the NAF to west, which is the transfer fault (Emre, Tüysüz, & Yıldırım, 2009; Yıldırım et al., 2013).

The strain due to the N-NW direction of the Arabian Plate is considered to cause uplift and crustal thickening in the Pontides, and this constriction continues to drive in the anti-clockwise direction of the Anatolian plate (e.g. McKenzie, 1972; Şengör, 1979). Accordingly, the Moho depth observed in the Eastern Pontides ranges from 42 to 46 km (Gök et al., 2016). The compressive structures can be seen in seismic profiles (TPAO; Robinson, Banks, Rutherford, & Hirst, 1995).

In the Eastern Pontides, between the Black Sea and the NAF, there are active faults in the North East Anatolian Fault (NEAF) and the thrust fault segments of this fault. As a conceptual model, the NAF transfer zone has multiple antithetic and synthetic faults (Badgley, 1965; Riedel, 1929; Vialon, Ruhland, & Grolier, 1976; Wilcox, Harding, & Seely, 1973). From these faults, NEAF is the antithetic fault of the NAF (e.g. Bektaş et al., 2001). According to a model by

Twiss and Moores (1992), the NEAF is a dextral strike-slip fault, which is bifurcated at places where the fault starts and ends. The dextral motion NEAF is approximately NE-oriented and inclined to move north to Bayburt and its vicinity.

The Borjomi Kazbegi Fault (BKF), with a NE-SW trend that is about 250 km length which forms the southwest segment of the North East Anatolian Fault zone that is about 800 km in length. The BKF is concave shaped, with a north-dipping thrust fault (Figure 2a). Besides, the Borjomi-Kazbegi Fault, which accompanies the uplift of the Pontides, is an active segment linked with the NEAF (i.e. Westaway, 1994). The connection between NEAF and NAF is accompanied by, 400 km long NE-SW trending and south-dipping Black Sea Fault (BSF). Seismic activity is more active in the NE of BSF than the SW of BSF.

In addition to the thrust faults, which are accommodated by the uplift in the Eastern Pontides, there are normal faults with many of the listric geometries dipping northward along the coastal parts of the Pontides (e.g. Yılmaz, 2017). The East Black Sea Fault Zone (EBSFZ) is composed of 65-km long en-echelon distributed fault zone which forms southern margin of the Black Sea (Figure 3). Most of the normal fault systems, characterized by overstepping and linked segments, display high angle scarps with en-echelon morphology (Bozkurt & Sözbilir, 2006; Ferrill, Stamatakos, & Sims, 1999). The similar geometry was also defined by Yılmaz (2017) around the eastern coast part of Eastern Pontides. The normal faults along the coast are also observed in the seismic sections and control the coastal morphology, the mountain fronts and triangular facets (Figs. 3 and 4).

In the seismic sections, a thrust fault occurred after the Miocene rocks around Rize (Robinson et al., 1995), and young sediments were folded around the Rioni Kura basin (Banks, Robinson, & Williams, 1997). This outcome was not the case on two sides of the same fault, but because they occurred on the same mechanism linked with NAF, the data show that the progressive uplift on the Eastern part of the Eastern Pontides is higher than that on the western part. When seismic activities are examined in the Eastern Pontides, three earthquakes of (i) 5.5, (ii) 5.3 and (iii) 4.2 magnitude are observed in the sea, and focal mechanism solutions of these faults are thrust faults near Batumi in 2012, 1959 and Trabzon region 2008, respectively.

4. Methods

In this study, the morphology of the mountain fronts of the northern part of the Eastern Pontides along the Black Sea coast and profiles of the longitudinal river were investigated. Geomorphic indices such as Hypsometric Integral (HI)-Hypsometric Curve (HC) (Keller & Pinter, 2002), Mountain Front Sinuosity (S_{mf}) (Bull & McFadden,

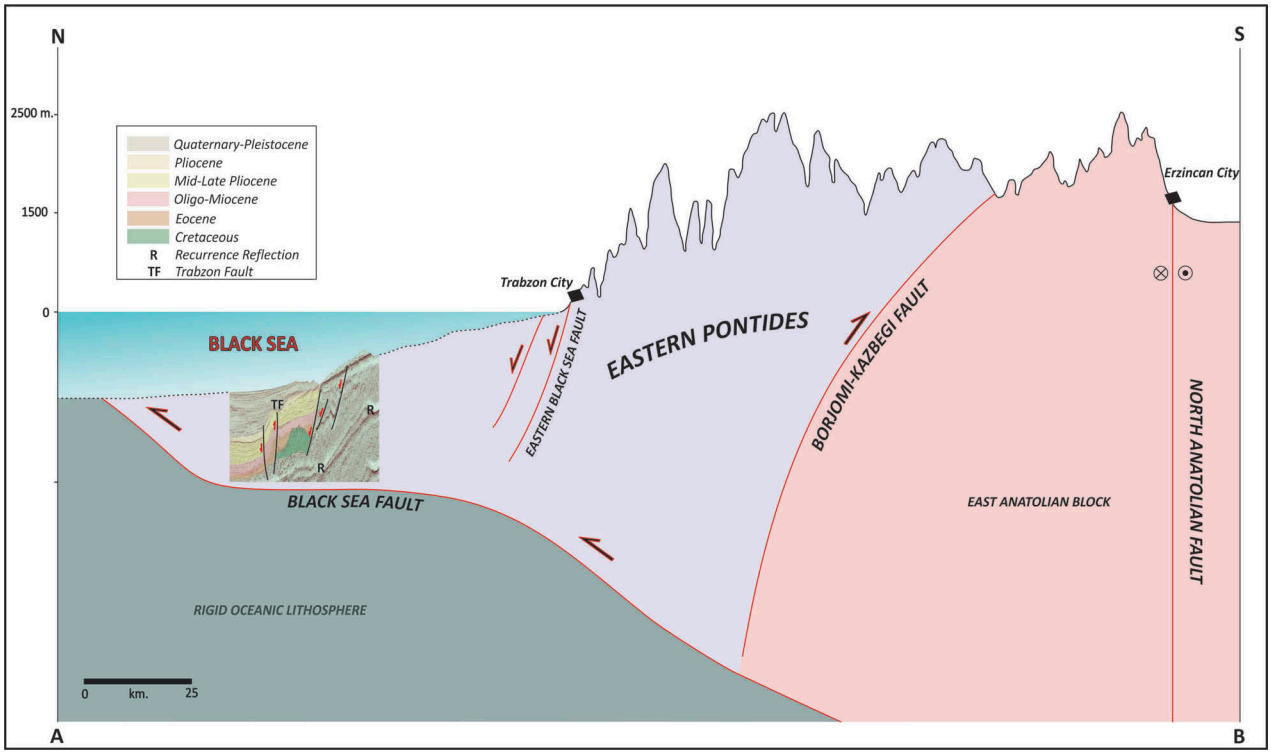


Figure 4. Schematic cross section with seismic profile from South to North. The location is shown with dashed line in Figure 2a. Onshore seismic profile located north of the Trabzon region (redrawn from Gündüz, 2015) showing active deformation of the Quaternary to Miocene levels.

1977), Valley Floor Width-to-Height Ratio (V_f) (Bull & McFadden, 1977), Stream Length Gradient Index (Hack-S_L) (Hack, 1973), Asymmetry Factor (AF) (Hare & Gardner, 1985), and Basin Shape Analyses (B_s) (Cannon, 1976) were carried out to clarify the tectonic evolution of the region between Trabzon and Rize, which is located on the coastal regions of the northeastern Pontides. The 1/25 000 scale topographical maps used were digitized from the General Command of Mapping (Turkey), and 1/25 000 scale geological maps were produced in the field; additionally, 1/100 000 scale geological maps were used by the General Directorate of Mineral Research and Explorations of Turkey.

4.1. *Rock strength and climate*

According to the rock groups and field studies in the study area, tectonic geomorphological evaluation of the study area was performed considering the strength ratings of the rock groups in the footwall and hanging walls along the fault zones, which were thought to be active on the mountain fronts of the Eastern Pontides. To standardize the rock strength (Selby, 1980), the following classification was used, in a manner similar to those in studies by e.g. Alipoor, Poorkermani, Zare, & El Hamdouni, (2011); El Hamdouni et al., (2008). In determining the strength of the rocks in the region, we used the derived from the rock unit and cementation type of the rocks such as those that are more resistant to weathering and marine erosion. The Eastern Pontides is one of the highest-volume precipitation areas of the world, where the processes of weathering and erosion are efficient. Rock strength and climate can generate higher debris shoots and can cause landslides in the drainage basin.

4.2. *Mountain front sinuosity*

The morphometric expression of the mountain fronts controlled by the faults was defined as $S_{mf} = L_{mf}/L_s$. Here, L_{mf} is the distance between the straight line between the two contour lines to be studied, and L_s is the net distance along the same contour interval (Bull & McFadden, 1977). S_{mf} is indicative of erosion and tectonic activity, and the S_{mf} value is related to the uplift in the region (Rockwell, Keller, & Johnson, 1984). When erosional processes work together with tectonic activity, the mountain fronts have wider and more sinusoidal structures (Bull & McFadden, 1977). Tectonically active sites usually have low S_{mf} ratios (1–1.5). If the S_{mf} values are > 3, the mountain fronts in this region are largely affected by erosional processes. If the value is > 3, active faults or intense tectonism on the mountain front is at least 1 km away from the current erosional processes (Bull, 2007; Bull & McFadden, 1977; Silva et al., 2003). In this study, S_{mf} values were calculated for nine fault-controlled mountain front along the EBSFZ.

4.3. *Valley floor width to height ratio*

The equation $V_f = -2\,V_{fw}/(E_{ld}\text{-}E_{sc}) - (E_{rd}\text{-}E_{sc})$ was used to quantify that the formation and development of the valleys are related to tectonics. Here, V_{fw} is the width of the valley basin, and E_{ld} and E_{rd} show the height of the eastern and western watershed, respectively, looking downstream in the drainage basin. Esc expresses the height of the floor of the valley (Bull & McFadden, 1977). Higher V_f values commonly refer to the formation of U shaped valleys, while lower V_f values indicate that the active tectonics play an important role in the formation and development of V shaped valleys (Bull & McFadden, 1977; Peréz-Peña, Azor, Azañon, & Keller, 2010; Rockwell et al., 1984; Silva et al., 2003). The transverse valley profiles which used to determine V_f are located ~ 250 m upstream of the mountain front for smaller drainage basins, and in large drainage basins, the valley profiles are located at ~ 250 and ~ 500 m upstream of the mountain front, in a manner similar to those in studies by e.g. Ramírez-Herrera (1998), Tsodoulos, Koukouvelas, & Pavlides (2008), Bull (2007), Özkaymak and Sözbilir (2012).

4.4. *Stream length gradient index*

$S_L = (\Delta_h/\Delta_L) * l$ was used for the numerical expression of the response given by the study area to rock strength and active tectonic processes. Here, Δ_h/Δ_L is the ratio between the height and the length of the channel or valley, and l is the length of the section up to the midpoint of the drainage area (Hack, 1973). S_L is calculated every 10 meters in topographical parameters. The S_L index is one of the most commonly used methods to determine the relative degree of activity of the studied region (Alipoor et al., 2011; Keller & Pinter, 2002; Troiani & Della Seta, 2008). In this analysis, it was determined that the effect tectonic and lithological controls on river profiles across the fault zones. The valley profiles were interpreted along 12 rivers that reached the mountain front in the study area and were controlled tectonically.

4.5. *Asymmetry factor*

$AF = (A_r/A_t) * 100$ was used as one of the numerical determinations of the relation between the drainage basins and the tectonic effect. Here, A_r is the sum of the area remaining on the right side of the flow direction of the river, and A_t represents the total drainage area. The Asymmetry Factor is one of the methods used to elucidate the formation of drainage basin and the state of tectonic control in its development (Cox, 1994; Hare & Gardner, 1985). According to this equation, the basin is asymmetric for values bigger and smaller than 50, and the basin is balanced if it is close to 50. If the value is less than 50, the basin is close to the right. If it is bigger than

50, it is close to the left (Scotti, Molin, Faccenna, Soligo, & Casas-Sainz, 2014). Peréz-Peña et al. (2010) uses the scales that are obtained by subtracting the value obtained from the asymmetry factor from 50 values. On this scale, AF < 5, symmetric; AF = 5–10, Light asymmetric; and AF = 10–15, Medium asymmetric. If AF> 15, it is mostly considered as an asymmetric basin.

Also, AF values can be divided into 3 main groups as follows: 45 < AF < 55 (Symmetric basin), AF> 55 (Asymmetric-orientated eastward basin), and AF < 45 (Asymmetric-oriented westward basin) (Özkaymak & Sözbilir, 2012).

4.6. *Hypsometric curve and hypsometric integral*

The equation HI = $(h_{mean}-h_{min})/(h_{max}-h_{min})$ was used in the numerical determination of the effect of tectonic on the drainage basins. The hypsometric curve and the hypsometric integral often measure relative availability and competence of the drainage basin. The hypsometric curve and the hypsometric integral are tools by which the drainage basin changes under tectonic, climatic and lithological factors (Hurtez, Sol, & Lucazeau, 1999; Willgoose & Hancock, 1998). Since the shape and height of the drainage basin do not affect the hypsometric curve, basins of different sizes can be compared with each other using a Hypsometric curve (Keller & Pinter, 2002; Strahler, 1952). The values were obtained from the analysis range from 0 to 1. When the HI values are close to 1, they signify young surfaces associated with active tectonics, while values close to 0 emphasize tectonically stagnant, aged and eroded surfaces.

4.7. *Basin shape geometry*

The geometry of the drainage basins, which shows the B_s value, is represented by the ratio B_l/B_w according to the ratio of the length of a drainage basin to its maximum width (Cannon, 1976; Ramírez-Herrera, 1998). Here, Bl is the basin length, and B_w represents the width of the widest point of the basin. The high values of the index indicate that they have longitudinal geometry and high values can be interpreted as the result of tectonic deformation (Bull & McFadden, 1977; Burbank & Anderson, 2001; Ramírez-Herrera, 1998).

5. Results

5.1. *Rock strength and climate*

Along the fault zone, the mountain front and hanging wall consist of sedimentary rocks such as alluvium, sandstone, conglomerate, and volcanic rocks such as basalt, andesite, rhyolite, and dacite. In the study area, the rocks were divided into the following 5 different strengths: very low (alluvium units), low (conglomerate), moderate (sandstone, tuff), high (basalt, andesite, rhyolite and dacite), and very high (Granite, Schist, Fillite, Gneiss) (Figure 3). These rocks are scattered in the mountain front, and the vicinity can be categorized as a very low, low, and moderate (Figure 5). Very high and high strength rocks do not show up in mountain fronts. According to the Figure 5, the mountain fronts that are 5 and 7 have very low rock strength, and the other mountain fronts have low-moderate rock strength. According to this index result, high and very high rock strength groups were observed along the southern zones of the Eastern Pontides rather than at the mountain fronts.

5.2. *Mountain front sinuosity*

Mountain front sinuosity values range from 1.2 to 1.5 (Table 1). In particular, all areas considered (from 1 to 9) have topographical signatures that indicate tectonic activity. When the Eastern-central and western parts of the Eastern Pontides are evaluated as a whole, almost all the areas have at moderate to high S_{mf} values. The S_{mf} values are the highest values in mountain front 9, while the lowest values are in mountain fronts 2 and 3. In this analysis of the coastal areas of the Eastern Pontides, the fault-controlled mountain fronts and their values follow a uniform trend (Figure 6).

5.3. *Valley floor width to height ratio*

The mean V_f values range from 0.4 to 1.2 (Table 1). According to these values and valley profiles, most of the valleys are in a transition between the V and U forms. As a result of the analyses, it was observed that the S_{mf} and V_f results were in harmony (Figure 6). In addition, there is a noticeable decrease in V_f values in the front of mountain fronts 2 and 8. This consistency between the S_{mf} and V_f values and the change of the V_f values relative to the morphology makes it reasonable to use these two indices to classify the relative tectonic activity of the region.

5.4. *Stream length gradient index*

According to Figure 7, Hack Index values range from 30 to 120. The minimum values are observed at the top of the hanging wall block, and alluvium in the mountain front is the top of the drainage basins in the footwall block. The S_L index between these two values increases and decreases according to the lithology and tectonic effect. The S_L profile of a river is considerably higher than that in low areas. However, when the spatial distribution of the S_L index is considered, it shows a different feature near the fault zones in the mountain front. Especially along the fault zones,

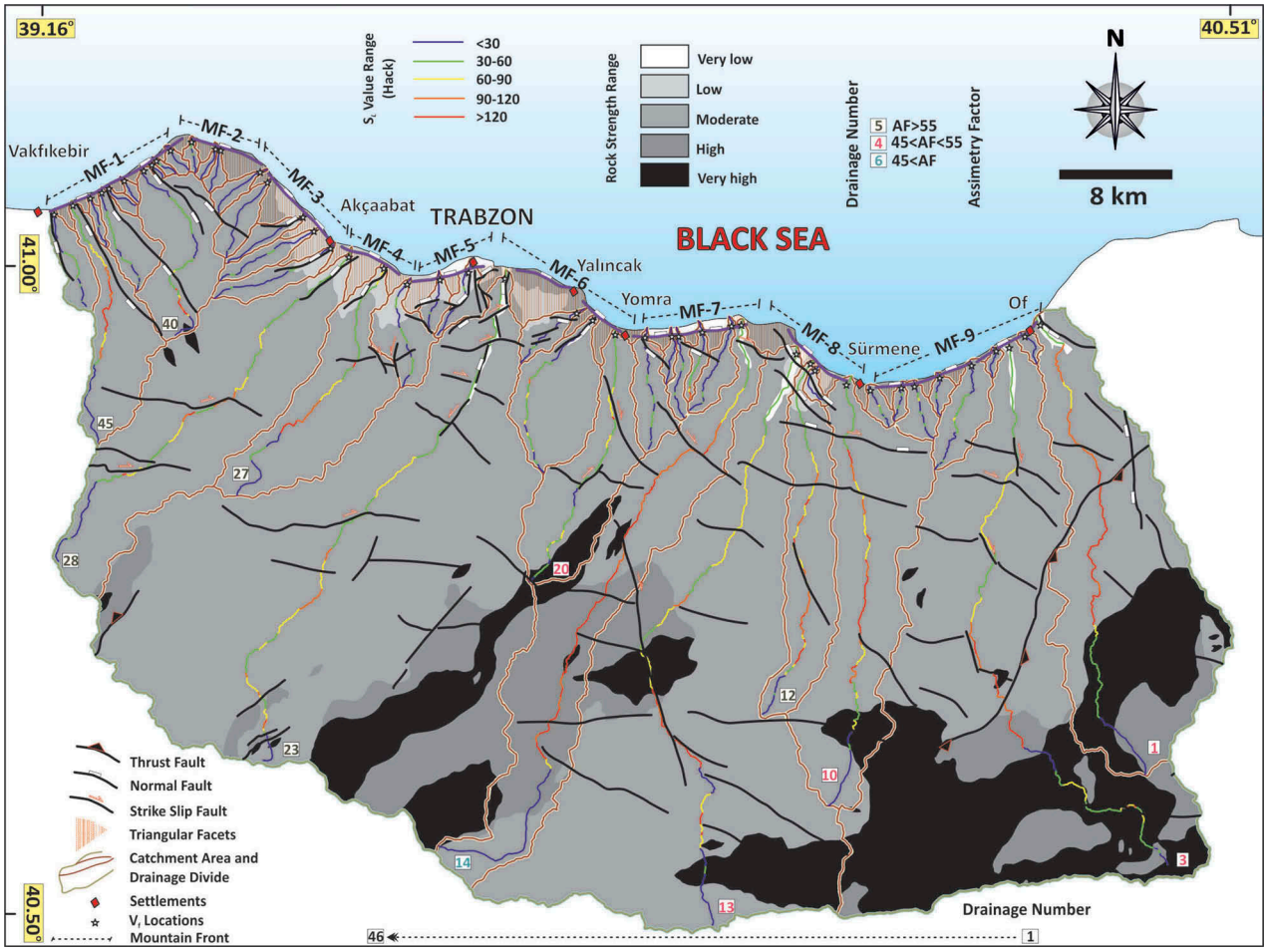


Figure 5. S_L indexes along the main channels and rock strength levels (according to Selby, 1980) of the study area. Rectangular box indicates the calculated catchments that distribution of the S_L index anomalies. AF values are indicated by pink, olive and green numbers scales in the box.

mountain fronts 5, 7, 8 and 9 indicate that the rivers have a very high gradient. In addition to the spatial distribution of the S_L index, S_L values were assessed by considering lithological factors in the longitudinal valley profiles (Figure 7). Accordingly, the longitudinal valley profiles clearly show the influence of the faulting on their geometries. Each river has a knickpoint, which corresponds to fault zones detected in the field. When the longitudinal valley profiles and the S_L index were evaluated together, each river was affected by more than one synthetic fault sloping northward and showed that the zone was tectonically active. At the same time, the S_L values reaching high values and having knickpoints indicate that the drainage basins that were analyzed are disequilibrium and transient character of the landscape due to progressively uplifting.

5.5. *Asymmetry factor*

Similar to Hare and Gardner (1985), asymmetry factor values in this study range from 35 to 81 (Table 1). These values are respectively; 61% of the AF values reflect an asymmetric basin pattern, while 39% indicate a symmetrical basin (Figure 5). In addition, the AF values were classified into four different categories, and many of the drainage basins were carrying asymmetrical deformation patterns as follows: light asymmetric (26.1%), moderate asymmetric (28.2%) and mostly asymmetric (6.5%).

5.6. *Hypsometric curve and hypsometric integral*

According to the Hypsometric curves analyses, the drainage basins show a profile with the ridges trending slightly to the NW and slightly to the NE. Starting from the east to the west of the Eastern Pontides, the profile is numbered from P1 to P46. All the analyzed drain basins are controlled by faults to the north. In the calculation and interpretation of the hypsometric indices, the tectonic effect is taken into consideration, as well as the lithological factors that remain in the drainage basin. In addition to the results, hypsometric integral values range from 0.37 to 0.67 (Table 1). HI values between 0.57 and 0.67 have hypsometric curves with a convex shape. The HI values of the drainage basins with the concave shape of the hypsometric curves range from 0.37 to 0.47. The drainage

Table 1. Morphometric parameters of the studied catchments and mountain fronts. HI: Hypsometric Integral, B_s: Basin Shape, AF: Asymmetry Factor (a) Hare and Gardner (1985); (b) Peréz-Peña et al. (2010), V_f: Valley Height-Valley Width (c) Mean V_f Values; (d) Sigma value is referring to 1 standard deviation of the full range of V_f values, S_{mf}: Mountain Front Sinuosity.

	Drainage Name	HI	B_s	AF [a]	AF [b]	V_f	V_f [c]	σn-1 [d]	S_{mf}
MF 9 (Mountain Front)	P1	0.53	2.59	45	5	1.31	0.89	0.44	1.25
	P2	0.65	2.01	46	4	0.94			
	P3	0.49	1.52	54	4	1.75			
	P4	0.63	2.53	55	5	1.02			
	P5	0.43	2.33	62	12	0.41			
	P6	0.5	1.95	58	8	0.41			
	P7	0.52	1.50	52	2	0.89			
	P8	0.51	3.29	58	8	0.28			
	P9	0.5	2.35	53	3	0.98			
	P10	0.49	4.01	55	5	0.93			
MF 8	P11	0.65	2.06	54	4	1.67	1.09	0.34	1.15
	P12	0.41	6.22	63	13	1.22			
	P13	0.63	1.59	51	1	1.57			
	P14	0.5	7.12	43	7	0.91			
MF 7	P15	0.37	3.10	64	14	0.78	1.23	0.52	1.15
	P16	0.39	3.84	48	2	1.25			
	P17	0.42	4.51	56	6	1.75			
	P18	0.51	3.64	39	11	1.76			
	P19	0.42	2.75	51	1	1.54			
	P20	0.47	3.04	54	4	0.32			
MF 6	P21	0.41	1.83	65	15	1.15	1.16	0.26	1.36
	P22	0.58	2.33	38	12	0.77			
	P23	0.54	1.23	59	9	1.24			
	P24	0.42	2.24	48	2	1.5			
MF 5	P25	0.46	2.0	62	12	1.76	1.07	0.69	1.34
	P26	0.46	1.6	46	4	0.38			
MF 4	P27	0.52	3.16	64	14	0.42	1.01	0.41	1.28
	P28	0.46	3.17	57	7	1.29			
	P29	0.48	4.55	59	9	1.31			
MF 3	P30	0.45	5.06	54	4	0.6	0.53	0.19	1.31
	P31	0.44	3.71	35	15	0.87			
	P32	0.47	2.45	50	0	0.4			
	P33	0.52	2.57	44	4	0.36			
	P34	0.54	1.74	57	7	0.42			
MF 2	P35	0.56	2.76	36	14	0.41	0.35	0.15	1.37
	P36	0.62	1.64	37	13	0.15			
	P37	0.58	1.97	50	0	0.51			
MF 1	P38	0.59	2.41	54	4	0.19	0.61	0.44	1.44
	P39	0.67	2.56	62	12	0.43			
	P40	0.38	2.33	59	9	0.69			
	P41	0.5	1.96	62	12	0.37			
	P42	0.5	2.75	44	6	0.74			
	P43	0.38	2.20	77	27	1.78			
	P44	0.49	4.36	47	3	0.39			
	P45	0.64	3.32	81	31	0.46			
	P46	0.39	2.78	61	11	0.45			

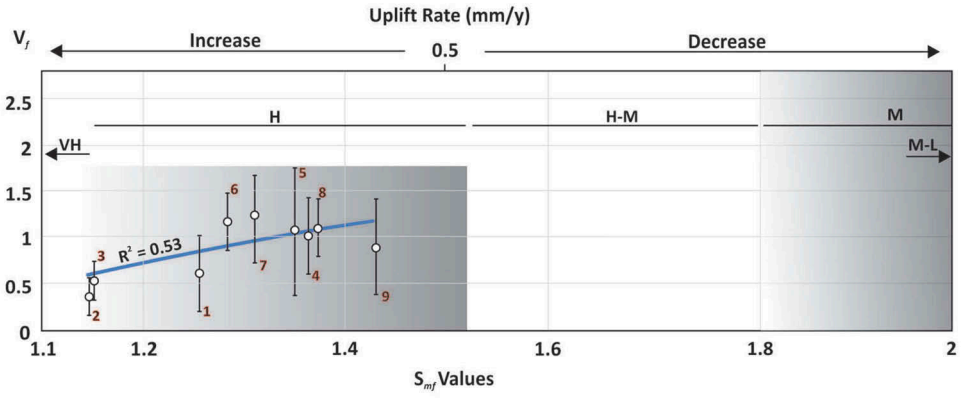


Figure 6. Plot of S_{mf} vs V_f for the mountain fronts of each segment and inferred activity classes. Vertical bars show the standard deviation (σn-1) for V_f values. Number at the top indicate inferred uplift rates U (mm/y) from Rockwell et al. (1984). VH: Very High, H: High, H-M: High to Moderate, M: Moderate, M-L: Moderate to Low.

basins, which have complex S-shaped hypsometric curves, have HI values ranging from 0.47 to 0.57 (Figure 8). In general, 21.8% of the hypsometric curves are convex, 30.4% are concave, and 47.8% are flat-S.

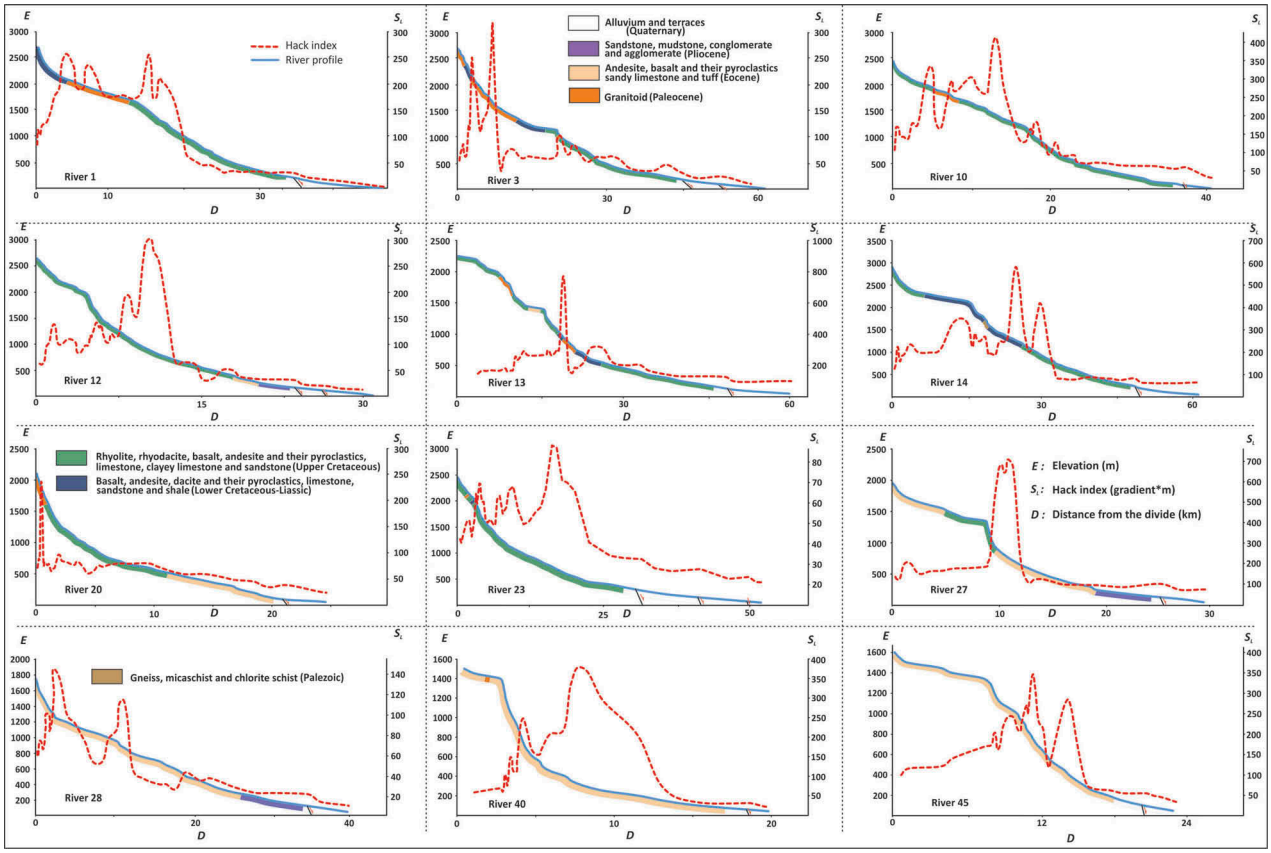


Figure 7. Longitudinal river profiles and measured S_L index values of the representative rivers that are not consecutively numbered. River numbers within the white boxes in Figure 5.

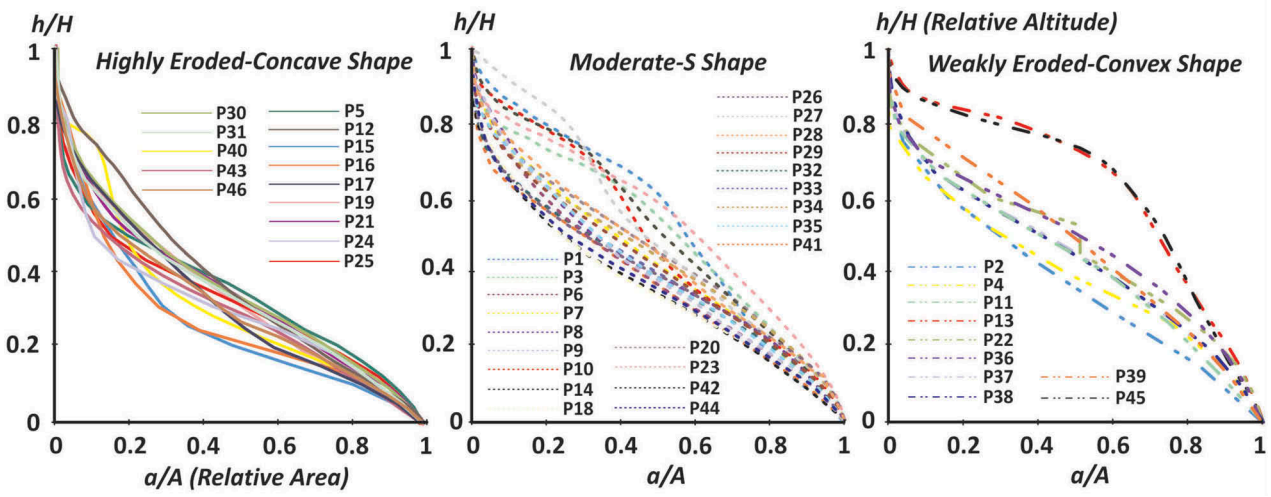


Figure 8. Hypsometry curves of 46 catchments along mountain fronts shown in Figure 5.

5.7. *Basin shape geometry*

The basin shape geometry was calculated for the 46 drainage basins. The B_s values in the study area range from 1.2 to 7, and when the size of the drainage basins in the region was taken into account, it was found that they had a longitudinal geometry (Table 1). Thus, a $B_s > 2$ has a longitudinal and narrow geometry reveal progressively uplifting.

6. Discussion

6.1. *Tectonic activity of the mountain front based on geomorphologic indices*

In this study, the results of all geomorphological indices between Trabzon and Rize are synthesized to reveal the activities of the tectonically controlled mountain fronts. The analyses of Mountain front Sinuosity (S_{mf}), Asymmetry Factor (AF), Valley Floor

Width to Height Ratio (V_f), Hypsometric Curves (HC), Hypsometric integrals (HI), Basin Shape Analysis (B_s) and Stream Length Gradient (Hack-S_L) for Eastern Pontides were performed for first time, and show the characteristics of areas subjected to active uplift.

S_{mf} and V_f analyses were evaluated together, which make it uplift rate for each segment and possible activity class, and the results were compared with the regression analysis (R) and found to be good at 53% accuracy (Figure 6). Bull and McFadden (1977) classified tectonic activity as dependent on S_{mf} and V_f values and based on this study, V_f vs. S_{mf} plots of the mountain fronts which shows that the northern part of the Eastern Pontides remains active at high levels. For this reason, it is more meaningful to classify the relative tectonic activity of the region by considering S_{mf} value and V_f values together with geomorphological indices separately. In addition to findings by Rockwell et al. (1984), the region was found to be uplifting more than 0.5 mm per year (Figure 6).

Previous studies stated that the Eastern Pontides uplifts at rates ranging from 0.59 to 1 mm per year in Quaternary period (Softa et al., 2017). Yıldırım et al. (2013) stated that the Central Pontides uplifts 0.23 mm/yr, and the rate of uplift is higher than 0.23 for the Eastern Pontides when the morphology of the Central Pontides is considered compared to the Eastern Pontides. When both the morphological analyses and the rate of uplift were evaluated together, it was determined that the coastal section of the Eastern Pontides is highly active.

S_L values can show various anomalies in relation to changes in the rock strength encountered at the site where the lithology changes, while the values are quite low in areas with low rock strength and relatively low local elevation, giving high anomalies in active uplifted areas with faults (Keller & Pinter, 2002). Suddenly rising S_L values on rocks with low strength generally show active tectonic deformation (Yıldırım, 2014). The relationship between high peak S_L values and the geology of the areas below the valley profiles was assessed in conjunction with the geology below the longitudinal valley profiles. S_L values were suddenly increasing and decreasing irrespective of the rigidity of the lithologies. Because the observed mountain fronts generally have very low and low strength rocks, the S_L values have morphology data that can be active in the fault segment controlling each mountain front (Figure 7).

Tectonically controlled mountain fronts and wide triangular surfaces typically result in the collapse of the hanging block along the fault zone and the rapid uplift of the foot block (Burbank & Anderson, 2001). These structures are intensively observed between Trabzon and Rize in the coastal part of the Eastern Pontides. (Figure 5). The mountain fronts and wide triangular surfaces that develop under the control of active normal faults symbolize the remains of the foot block due to the differential uplifting related to tectonics (Wallace, 1978).

Even though Hypsometric Integral (HI) does not relate directly to relative active tectonics, HI values are affected by the rock strength and climate (El Hamdouni et al., 2008). According to HI results, the convex-shaped drainage basins with high HI values show that the rock strength groups in relatively high topographic areas have strength values varying from very low to very hard. These high values and convex curves show that there are traces of active tectonics in the current morphology of the region. S-shaped hypsometric curves considered as complex hypsometric curves showed that active tectonics and the lithological effect of the region cooperates with rejuvenation processes at the tip of the troughs in the drainage basin (Figure 8).

Taken into consideration the uniformity of the climatic conditions in the Eastern Pontides, the Hack index and HI results that generally reflect by both rock strength and climate, and drainage development and local geomorphology that are affected by the tectonic uplifting and region deformation suggest that climate may have significant impact on the studied deformation zone.

Drainage basins initially develop perpendicular to orientation of the deformation zone and progressively change the inclination along with ongoing deformation (Castelltort et al., 2012; Goren, Castelltort, & Klinger, 2015; Yıldırım & Tüysüz, 2017). Asymmetry factor (AF) is sensitive to change in drainage basins inclination perpendicular to the mean stream direction (El Hamdouni et al., 2008). Structural control of the bedding orientation may play a great role in the development of basin asymmetry in the progressively uplifting area (Alipoor et al., 2011). Except for eastern drainage basins (tectonically stable), the AF values for the middle and western drainage basins in the studied area indicate tilting and relative active uplifting (Figure 5). This finding suggests that the Eastern Pontides is mostly dominated by asymmetric basins. This asymmetry can be explained by push up structure linked with effect on the oblique movement of BKF and BSF thrust faults. Basin Shape Geometry (B_s) > 2 indicating that in these areas relative tectonic activities are higher than in others.

6.2. *The uplift model of the Eastern Pontides*

In addition to morphometric and field studies, previous studies have shown that the NAF is an important effect on the evolution of the Eastern Pontides, where has been drifting to the north due to the possible uplift mechanism (e.g. Sarıbudak, 1989a, 1989b; Hisarlı,

2011). The NAF transfers deformation to the northern part of the interior of the Anatolian plate. This observed deformation is distributed to the region between the Black Sea and the NAF. This active deformation is accommodated by thrust and normal faults observed in the field and seismic sections. These faults are thought to have inherited faults that have been active since Cenozoic times. These observed structures form the asymmetric topography of the Pontides accommodated the uplifting in the region.

The Eastern Pontides and the thrust faults along its southern and northern flanks are associated with the strike-slip North Anatolian Fault to the west and the NEAF to the east. Thrust faults with right-lateral movements along this push-up structure cause crustal shortening, so the thrust and strike-slip styles of faulting are intimately related. Given the tectonic structure of the Eastern Pontides, a plausible scenario is likely that the flattening of the underlying thrust at very shallow depths is probably responsible for the collapse of the thrust 'nose' by normal faulting (Bull, 2007; Kurushin et al., 1997). This type of normal faulting may be merged at depth on the main thrust fault (Figure 9).

The northern part of the Pontides is surrounded by active faults which is the Black Sea Fault, and the region has been continuing seismic activity with the 5.5, 5.3 and 4.2 earthquakes near Batumi in 2012, 1959 and Trabzon region 2008, respectively. At the same time, the fact that the focal mechanism solutions of these earthquakes are the thrust faults suggest that these earthquakes are on the Black Sea Fault, which is a south-dipping thrust fault.

Tectonic, geomorphologic and geologic studies, as well as seismic reflection profiles, were evaluated together and reveal that the area between the Black Sea and the NAF contributes is progressively uplifting with a push-up structure (Figure 9a).

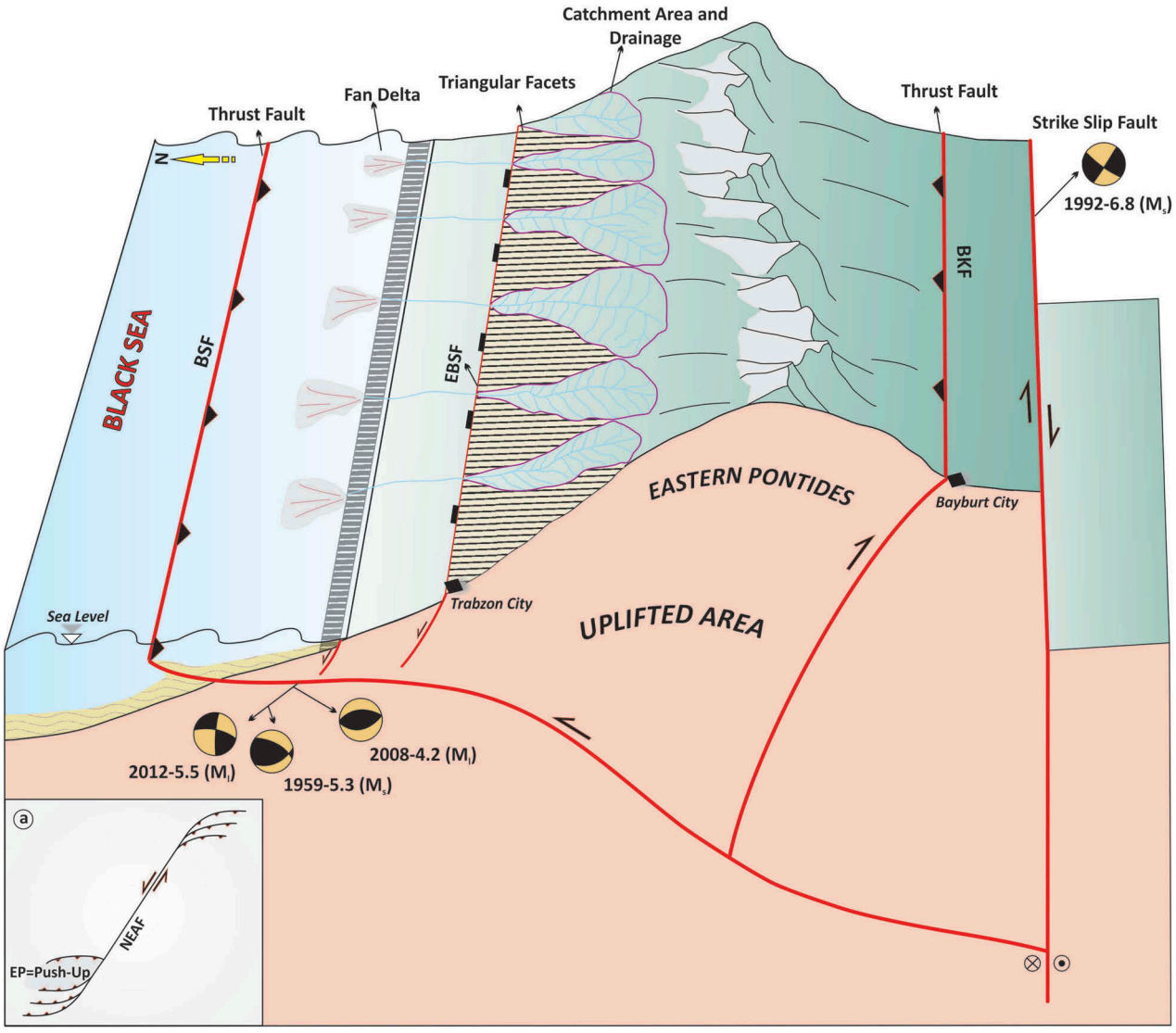


Figure 9. A conceptual model for the Eastern Pontides, which demonstrate an active deformation zone and has a 'push-up' geometry within the Black Sea Fault (BSF) in the sea and the Borjomi-Kazbegi Fault (BKF) on land in conjunction with the North Anatolian Fault (NAF) at depth. Dashed yellow areas are schematic representations of deformed Neogene deposits in the Trabzon region. (a) Sketch of the Eastern Pontides Push up structure (adapted from Twiss & Moores, 1992).

Regionally, the Eastern Pontides has been uplifted by the Black Sea Fault and the Borjomi-Kazbegi thrust faults, which are active segments of NEAF (i.e. Westaway, 1994), south-dipping in the Black Sea in the north and north-dipping in the south.

Along the coastal regions of the Eastern Pontides, the mountain range resembles that of the NAF. When the morphology of the Eastern Pontides was examined from north to south, there was an asymmetry between the south and the north. This asymmetric pattern can be explained by uplifting linked with the NAF effects in the Eastern Pontides and the spatial distribution of the faults on the land and in the sea, as well as their geometry.

6.3. *Evaluation of the seismic activity of the Eastern Pontides*

Currently, seismic risk studies mostly focus on both high seismic activity areas and high stress areas. In the northern part of the Eastern Pontides, stress accumulation was intensified due to the N-S compression, and large magnitude earthquakes occurred in the sea. However, although the seismic risk studies carried out so far have been evaluated on land and near main fault zones, active faults at the sea have been excluded.

Active deformation zones are the sites of low, moderate and high earthquake activity linked with rapid vertical movement in this region. Over the three hundred earthquakes that were greater than a magnitude of 3 were detected using catalogs of instrumental and historical earthquakes between 1852 and 2018. Seismic activity in the study area is shown in Figure 2a, b, and is dominated by thrust-faulting earthquakes, many of which show a low-angle, south-dipping fault plane consistent with northerly motion on the main subduction margin in the Eastern Pontides. In contrast to the widespread thrust-faulting earthquakes, normal-faulting mechanisms don't seem in these earthquakes.

Çifçi, Dondurur, and Ergun (2002), defined creep structures in the seabed using the seismic profiles in Trabzon area. Fault segments that actively creep are often delineated by small earthquakes, some of which appear to regularly repeat in time and location (e.g. Nadeau, Foxall, & McEvilly, 1995; Rau, Chen, & Ching, 2007).

While large earthquakes don't seem in the in this region, our uplift rate indicates that result is over the 0.5 mm/yr (Figure 6); this event can be explained fault creep. Stress accumulation due to the N-S compression in response to large earthquakes on the thrust faults in the Eastern Pontides. Because of the fault creep, many of small earthquakes are often seem in the Eastern Pontides.

Seismic risk assessments have been made in previous studies (e.g. Demircioğlu et al., 2017; Akkar et al. 2018) and the region between the NEAF and the NAF in the south of the Eastern Pontides was assessed in the medium to high risk group.

Given the uplift rates (e.g. Softa et al., 2017) the expression of moderate to high stress to the north of the Eastern Pontides does mean that the seismic assessment in this region will be compatible with this study. Our studies of morphometric analysis and earthquakes, especially in the sea, show that this region currently has high activity (Figure 6). The results obtained in morphometric studies of mountain fronts are meaningful when combined with other studies in the region.

Based on this assessment, the seismic value of the zone was evaluated together with the results of the morphometric analysis, seismic reflection profiles, regional stress distribution maps, and GPS data, and the Eastern Pontides show that medium-large magnitudes earthquakes continue within the high regions in terms of seismicity in the last 20 years.

7. Conclusion

The hypsometric curve-hypsometric integral results applied to the drainage basins along with the geomorphological indices and gradient analyses of the tectonically controlled mountain fronts were tectonically active in the Eastern Pontides, and the tectonic levels were relatively high when evaluated according to the S_{mf} and V_f analyses of the region. The results show that the seismicity of the Eastern Pontides is in harmony with the small to large earthquakes that occur on the land and in the sea. However, aseismic creep can be prevented too large earthquakes from occurring. The compressing of the Arabian plate throughout the N-S region was transmitted to the Eastern Pontides, where the stress was accommodated by thrust faults and normal faults with listric geometry. According to our conceptual model, the Eastern Pontides have been gradually uplifting in the 'push-up' geometry of the Black sea Fault and the Borjomi-Kazbegi faults linked with the NAF since the Late Quaternary period.

Acknowledgments

This work is part of a Ph.D. thesis undertaken by Mustafa SOFTA (MS) at the Institute of Natural and Applied Sciences, Dokuz Eylül University, Turkey. This study is funded by Dokuz Eylul University Research Projects "DEU-BAP-2014. KB.FEN.044". MS was supported by The Scientific and Technological Research Council of Turkey (TUBITAK). We thank Sarah Boulton and an anonymous reviewer for their thorough and constructive reviews. The manuscript was edited by Elsevier Language Editing.

Disclosure statement

No potential conflict of interest was reported by the authors.

Funding

This work was supported by the Dokuz Eylül University [2014.KB.FEN.044];

ORCID

Mustafa Softa http://orcid.org/0000-0001-5064-9260
Tahir Emre http://orcid.org/0000-0002-2687-5265
Hasan Sözbilir http://orcid.org/0000-0002-3777-4830
Joel Q. G. Spencer http://orcid.org/0000-0003-1374-7253
Mehmet Turan http://orcid.org/0000-0001-9108-6695

References

Adamia, S. A., Lordkipanidze, M. B., & Zakariadze, G. S. (1977). Evolution of an active continental margin as exemplified by the Alpine history of the Caucasus. *Tectonophysics*, *40*, 183–189.

Akkar, S., Azak, T., Çan, T., Çeken, U., Demircioğlu-Tümsa, M. B., Duman, T. Y., & Zülfikar, Ö. (2018). Evolution of seismic hazard maps in Turkey. *Bulletin Earthquake Engineering*. https://doi.org/10.1007/s10518-018-0349-1

Alipoor, R., Poorkermani, M., Zare, M., & El Hamdouni, R. (2011). Active tectonic assessment around Rudbar Lorestan damsite, high Zagros belt (SW of Iran). *Geomorphology*, *128*, 1–14.

Avagyan, A., Sosson, M., Karakhanian, A., Philip, H., Rebai, S., Rolland, Y., … Davtyan, V. (2010). Recent tectonic stress evolution in the Lesser Caucasus and adjacent regions. In M. Sosson, N. Kaymakci, R. A. Stephenson, F. Bergerat, & V. Starostenko (Eds.), *Sedimentary Basin Tectonics from the Black Sea and Caucasus to the Arabian Platform* (pp. 393–408). London: Geological Society.

Badgley, P. C. (1965). *Structural and Tectonic Principles* (pp. 521). New York, N.Y: Harper.

Bagha, N., Arian, M., Ghorashi, M., Pourkermani, M., El Hamdouni, R., & Solgi, A. (2014). Evaluation of relative tectonic activity in the Tehran basin, central Alborz, northern Iran. *Geomorphology*, *213*, 66–87.

Banks, C. J., Robinson, A. G., & Williams, M. P. (1997). Achara Trialeti fold belt and the adjacent Riouni and Kartli foreland basins. In Republic of Georgia, A. G. Robinson (ed, *AAPG Memoir 68: Regional and Petroleum Geology of the Black Sea and Surrounding Region* (pp. 331–346). USA: AAPG.

Barka, A. A. (1992). The North Anatolian Fault Zone. *Annales Tectonicae*, *6*, 164–195.

Bektaş, O., & Çapkınoğlu, S. (1997). Neptunian dikes and block tectonics in the eastern Pontide magmatic arc, NE Turkey: Implications for the kinematics of the Mesozoic basins. *Geosound*, *30*, 451–461.

Bektaş, O., Çapkınoğlu, S., & Akdağ, K. (2001). Successive extensional tectonic regimes during the Mesozoic as evidenced by neptunian dikes in the Pontide Magmatic Arc, Northeast Turkey. *International Geology Review*, *43*(9), 840–849.

Bektaş, O., Şen, C., Atıcı, Y., & Köprübası, N. (1999). Migration of the upper cretaceous subduction related volcanism towards the Back-arc Basin of the Eastern Pontide Magmatic Arc (NE Turkey). *Geological Journal*, *34*, 95–106.

Bozkurt, E., & Sözbilir, H. (2006). Evolution of the large-scale active Manisa Fault, southwest Turkey: Implications on fault development and regional tectonics. *Geodinamica Acta*, *19*, 427–453.

Bull, W. B., & McFadden, L. D. (1977). Tectonic geomorphology north and south of the Garlock fault, California. In: D. O. Doehering (Ed.), *Geomorphology in arid regions*. Proceedings at the Eighth Annual Geomorphology Symposium (pp. 115–138). State University of New York, Binghamton, NY.

Bull, W. B. (1977). Tectonic geomorphology of the Mojave Desert: US, Geological Survey Contract Report 14-08-001-G-394, Office of Earthquakes, *Volcanoes, and Engineering* (pp.188). California: Menlo Park.

Bull, W. B. (2007). *Tectonic Geomorphology of Mountains: A New Approach to Paleoseismology* (pp. 316). Oxford: Wiley-Blackwell.

Burbank, D. W., & Anderson, R. S. (2001). *Tectonic Geomorphology*. Malden: Science. 274. (0-632-04386-5)

Cannon, P. J. (1976). Generation of explicit parameters for a quantitative geomorphic study of the mill creek drainage basin. *Oklahoma Geology Notes*, *36*(1), 3–16.

Castelltort, S., Goren, L., Willett, S. D., Champagnac, J. D., Herman, F., & Braun, J. (2012). River drainage patterns in the New Zealand Alps primarily controlled by plate tectonic strain, *Nat. Geoscicence*, *5*(10), 744–748.

Chorowicz, J., Dhont, D., & Adıyaman, Ö. (1998). Black Sea–Pontid relationship: Interpretationin terms of subduction. *Abstract of Third International Turkish Geology Symposium*, Ankara, 258.

Çifçi, G., Dondurur, D., & Ergun, M. (2002). Sonar and high resolution seismic studies in the Eastern Black Sea. *Turkish Journal of Earth Sciences*, *11*(1), 61–81.

Cox, R. T. (1994). Analysis of drainage-basin symmetry as a rapid technique to identify areas of possible Quaternary tilt-block tectonics: An example from the Mississippi Embayment. *Geological Society of America Bulletin*, *106*, 571–581.

Demircioğlu, M. B., Şeşetyan, K., Duman, T. Y., Çan, T., Tekin, S., & Ergintav, S. (2017). A probabilistic seismic hazard assessment for the Turkish territory: Part II—Fault source and background seismicity model. *Bulletin Earthq Engineering*. https://doi.org/10.1007/s10518-017-0130-x

Dewey, J. F., Pitman, W. C., Ryan, W. B. F., & Bonnin, J. (1973). Plate tectonics and evolution of the Alpine system. *Geological Society of America Bulletin*, *84*, 3137–3180.

Dewey, J. F., & Şengör, A. M. C. (1979). Aegean and surrounding regions: Complex multiplate and continuum tectonics in a convergent zone. *Geological Society of America Bulletin*, *90*, 84–92.

El Hamdouni, R., Irigaray, C., Fernández, T., Chacón, J., & Keller, E. A. (2008). Assessment of relative active tectonics, southwest border of the Sierra Nevada (southern Spain). *Geomorphology*, *96*, 150–173.

Emre, O., Tüysüz, O., & Yıldırım, C. (2009). Uplift of Pontide orogenic belt since the late Miocene, *Second International Symposium on the Geology of the Black Sea Region*, MTA Congress Centre, Ankara, Abstract book, (p. 66–67).

Eyuboglu, Y., Bektaş¸, O., & Pul, D. (2007). Mid-Cretaceous olistostromal ophiolitic melange developed in the back-arc basin of the eastern Pontide magmatic arc (NE Turkey). *International Geology Review*, *49*(12), 1103–1126.

Eyuboglu, Y., Bektaş, O., Seren, A., Maden, N., Jacoby, W. R., & Özer, R. (2006). Three-directional extensional deformation and formation of the Liassic rift basins in the eastern Pontides (NE Turkey). *Geologica Carpathica*, *57*(5), 337–346.

Eyuboglu, Y., Santosh, M., Bektaş, O., & Ayhan, S. (2011). Arc magmatism as a window to plate kinematics and subduction polarity: Example from the eastern Pontides belt, NE Turkey. *Geoscience Frontiers*, *2*(1), 49–56.

Ferrill, D. A., Stamatakos, J. A., & Sims, D. (1999). Normal fault corrugation: Implications for growth and seismicity of

active normal faults. *Journal of Structural Geology*, *21*, 1027–1038.

Fichtner, A., Saygin, E., Taymaz, T., Cupillard, P., Capdeville, Y., & Trampert, J. (2013). The deep structure of the North Anatolian fault zone. *Earth and Planetary Science Letters*, *373*, 109–117.

Gök, R., Mellors, R. J., Sandvol, E., Pasyanos, M., Hauk, T., Takedatsu, R., … Javakishvirli, Z. (2016). Lithospheric velocity structure of the Anatolian plateau-Caucasus-Caspian region. *Journal of Geophysical Research: Solid Earth*, *116* (B5), 2156–2202.

Goren, L., Castelltort, S., & Klinger, Y. (2015). Modes and rates of horizontal deformation from rotated river basins: Application to the Dead Sea fault system in Lebanon. *Geology*, *43*(9), 843–846.

Gündüz, S. (2015). *Investigation of Active Tectonism Structure of The Eastern Black Sea with Using Multichannel Seismic Data* (Unpublished master's thesis). Dokuz Eylül University, Izmir, Turkey.

Gürbüz, A., & Gürer, Ö. F. (2008). Tectonic geomorphology of the North Anatolian fault zone in the lake Sapanca Basin (eastern Marmara Region, Turkey). *Geosciences Journal*, *12*, 215–225.

Güven, I. H. (1993). *Geological and Metallogenic Map of the Eastern Black Sea Region; 1:250,000 Map*. Trabzon: General Directorate of Mineral Research and Exploration.

Hack, J. T. (1973). Stream-profile analysis and stream-gradient index. *Journal of Research of the U. S. Geological Survey*, *1*, 421–429.

Hare, P. W., & Gardner, T. W. (1985). Geomorphic indicators of vertical neotectonism along converning plate margins, Nicoya Peninsula, Costa Rica. In M. Morisawa & J. T. Hack (Eds.), *Tectonic geomorphology*. Proceedings of the 15th Annual Bighampton Geomorphology Symposium (pp. 75–104). Boston, MA: Allen&Unwin.

Hisarlı, Z. M. (2011). New paleomagnetic constraints on the late Cretaceous and early Cenozoic tectonic history of the Eastern Pontides. *Journal of Geodynamic*, *52*, 114–128.

Hurtez, J. E., Sol, C., & Lucazeau, F. (1999). Effect of drainage area on hypsometry from an analysis of small-scale drainage basins in the Siwalik Hills (Central Nepal). *Earth Surface Processes and Landforms*, *24*, 799–808.

Kadirioğlu, F. T., & Kartal, R. F. (2016). The new empirical magnitude conversion relations using an improved earthquake catalogue for Turkey and its near vicinity (1900–2012). *T Journal Earth Sciences*, *25*, 303–310.

Kahle, H. G., Cocard, M., Peter, Y., Geiger, A., Reilinger, R., Barka, A. A., & Veis, G. (2000). GPS-derived strain rate field within the boundary zones of the Eurasian, African, and Arabian Plates. *Journal of Geophysical Research*, *105*, 23353–23370.

Keller, E. A. (1986). Investigation of active tectonics: Use of surficial earth process. In R. E. Wallace (Ed.), *Active tectonics* (pp. 136–147). Washington, DC: National Academy press.

Keller, E. A., & Pinter, N. (2002). *Active Tectonics: Earthquakes, Uplift, and Landscape* (pp. 362). NJ: Prentice Hall, Upper Saddle River.

Keskin, S., Pedoja, K., & Bektaş, O. (2011). Coastal uplift along the eastern Black Sea coast: New marine terrace data from eastern Pontides, Trabzon (Turkey) and a review. *Journal of Coastal Research*, *27*, 63–73.

Kurushin, R. A., Bayasgalan, A., Ölziybat, M., Enkhtuvshin, B., Molnar, P., Bayarsayhan, C., … Lin, J. (1997). The surface rupture of the 1957 Gobi-Altay, Mongolia, earthquake, Geological Society of America, Colorado, p. 320.

Mayer, L. (1986). Tectonic geomorphology of escarpments and mountain fronts. In R. E. Wallace (Ed.), *Active tectonics, Studies in Geophysics* (pp. 125–135). Washington, DC: National Academy Press.

McKenzie, D. (1972). Active tectonic of the Mediterranean region. *Geophysical Journal of the Royal Astronomical Society*, *30*, 109–185.

McKenzie, D. (1978). Active tectonics of the Alpine–Himalayan belt: The Aegean Sea and surrounding regions. *Geophysical Journal of the Royal Astronomical Society*, *55*, 217–254.

Nadeau, R., Foxall, W., & McEvilly, T. (1995). Clustering and periodic recurrence of microearthquakes on the San Andreas fault at Parkfield, California. *Science*, *267*, 503–507.

Özkaymak, Ç., & Sözbilir, H. (2012). Tectonic geomorphology of the Spildağı high ranges, western Anatolia. *Geomorphology*, 173–174, 128–140.

Özkaymak, Ç. (2015). Tectonic analysis of the Honaz Fault (western Anatolia) using geomorphic indices and the regional implications. *Geodinamica Acta*, *27*, 110–129.

Pavano, F., Pazzaglia, F. J., & Catalano, S. (2016). Knickpoints as geomorphic markers of active tectonics: A case study from northeastern Sicily (southern Italy). *Lithosphere*, *8*(6), 633–648.

Peréz-Peña, J. V., Azor, A., Azañon, J. M., & Keller, E. A. (2010). Active tectonics in the Sierra Nevada (Betic Cordillera, SE Spain): Insights from geomorphic indexes and drainage pattern analysis. *Geomorphology*, *119*, 74–87.

Ramírez-Herrera, M. T. (1998). Geomorphic assessment of active tectonics in the Acambay graben, Mexican Volcanic Belt. *Earth Surface Processes and Landforms*, *23*, 317–332.

Rau, R.-J., Chen, K. H., & Ching, K.-E. (2007). Repeating earthquakes and seismic potential along the northern Longitudinal Valley fault of eastern Taiwan. *Geophys. Res. Lett.*, *34*, L24301.

Reilinger, R., McClusky, S., Vernant, P., Lawrence, S., Ergintav, S., Çakmak, R., … Karam, G. (2006). GPS constraints on continental deformation in the Africa-Arabia-Eurasia continental collision zone and implications for the dynamics of plate interactions. *Journal of Geophysical Research. 111* (B5), B05411.

Reilinger, R., McClusky, S. C., Oral, M. B., King, R. W., Toksöz, M. N., Barka, A. A., … Sanlı, I. (1997). Global positioning system measurements of present-day crustal movements in the Arabia- Africa-Eurasia plate collision zone. *Journal of Geophysical Research*, *102*, 9983–9999.

Riedel, W. (1929). Zur mechanik geologischer brucherscheinungen. Zentralblatt für Mineralogie. *Geologie Und Paläontologie*, *1929*(B), 354.

Robinson, A. G., Banks, C. J., Rutherford, M. M., & Hirst, J. P. P. (1995). Stratigraphic and structural development of the Eastern Pontides, Turkey. *Journal of the Geological Society*, *152*, 861–872.

Rockwell, T. K., Keller, E. A., & Johnson, D. L. (1984). Tectonic geomorphology of alluvial fans and mountain fronts near Ventura, California. In: M. Morisawa (Ed.), *Tectonic Geomorphology*. Proceedings of the 15th Annual

Geomorphology Symposium. (pp. 183–207). Allen and Unwin Publishers, Boston, MA.

Rolland, Y., Hassig, M., Bosch, D., Meijers, M. J. M., Sosson, M., Bruguier, O., … Sadradze, N. (2016). A review of the plate convergence history of the East Anatolia-Transcaucasus region during the Variscan: Insights from the Georgian basement and its connection to the Eastern Pontides. *Journal of Geodynamics*, *96*, 131–145.

Sarıbudak, M. (1989a). A paleomagnetism approach to the origin of the Black Sea. *Geophysical Journal International*, *99*, 247–251.

Sarıbudak, M. (1989b). New results and palaeomagnetic overview of the Pontides in northern Turkey. *Geophysical Journal International*, *99*(3), 521–531.

Scotti, V. N., Molin, P., Faccenna, C., Soligo, M., & Casas-Sainz, A. (2014). The influence of surface and tectonic processes on landscape evolution of the Iberian Chain (Spain): Quantitative geomorphological analysis and geochronology. *Geomorphology*, *206*, 37–57.

Selby, M. J. (1980). A rock strength classification for geomorphic purposes: With tests from Antarctica and New Zealand. *Zeitschrift Für Geomorphologie*, *24*, 31–51.

ŞEngör, A. M. C. (1979). The North Anatolian transform fault: Its age, offset and tectonic significance. *Journal Of. Geological Society*, *136*, 269–282.

ŞEngör, A. M. C., Özeren, S., Keskin, M., Sakınç, M., Özbakır, A. D., & Kayan, I. (2008). Eastern Turkish high plateau as a small Turkic-type orogen: Implications for post-collisional crust-forming processes in Turkic-type orogens. *Earth Science Review*, *90*(1–2), 1–48.

ŞEngör, A. M. C., & Yılmaz, Y. (1981). Tethyan evolution of Turkey: A plate tectonic approach. *Tectonophysics*, *75*, 181–241.

Silva, P. G., Goy, J. L., Zazo, C., & Bardají, T. (2003). Fault-generated mountain fronts in southeast Spain: Geomorphologic assessment of tectonic and seismic activity. *Geomorphology*, *50*, 203–225.

Softa, M., Spencer, J. Q. G., Emre, T., Sözbilir, H., & Turan, M. (2017). Late Quaternary Rapid Uplift Deduced from Marine Terraces in Eastern Pontides, Turkey. *Geological Society of America Abstracts with Programs*, *49*(6). doi:10.1130/abs/2017AM-305129

Sosson, M., Rolland, Y., Danelian, T., Muller, C., Melkonyan, R., Adamia, S., … Galoyan, G. (2010). Subductions, obduction and collision in the Lesser Caucasus (Armenia, Azerbaijan, Georgia), new insights. *Geological Society of London, Special Publications*, *340*, 329–352.

Strahler, A. N. (1952). Hypsometric (area-altitude) analysis of erosional topography. *Geological Society of America Bulletin*, *63*, 1117–1141.

Taymaz, T., Yılmaz, Y., & Dilek, Y. (2007). The geodynamics of the Aegean and Anatolia: Introduction, in The Geodynamics of the Aegean, Anatolia. *Geological Society London, Special Publications*, *291*, 1–16.

Tepe, Ç., & Sözbilir, H. (2017). Tectonic geomorphology of the Kemalpaşa Basin and surrounding horsts, southwestern part of the Gediz Graben, Western Anatolia. *Geodinamica Acta, 29(1)*, 70–90.

TPAO (http://www.tpao.gov.tr)

Troiani, F., & Della Seta, M. (2008). The use of the stream length-gradient index in morphotectonic analysis of small catchments: A case study from Central Italy. *Geomorphology*, *102*, 159–168.

Troiani, F., Galve, J. P., Piacentini, D., Della Seta, M., & Guerrero, J. (2014). Spatial analysis of stream length-gradient (SL) index for detecting hillslope processes: A case of the Gállego River headwaters (Central Pyrenees, Spain). *Geomorphology*, *214*, 183–197.

Tsereteli, N., Tibaldi, A., Alania, V., Gventsadse, A., Enukidze, O., Varazanashvili, O., & Müller, B. I. R. (2016). Active tectonics of central-western Caucasus, Georgia. *Tectonophysics*, *691*, 328–344.

Tsodoulos, I. M., Koukouvelas, I. K., & Pavlides, S. (2008). Tectonic geomorphology of the easternmost extension of the Gulf of Corinth (Beotia, Central Greece). *Tectonophysics*, *453*, 211-232. doi:10.1016/j.tecto.2007.06.015

Twiss, R. J., & Moores, E. M. (1992). *Structural Geology* (pp. 531). New York: W.H. Freeman and Company.

Ustaömer, T., & Robertson, A. H. F. (1996). Paleotethyan tectonic evolution of the north Tethyan margin in the central Pontides, N Turkey. In: A. Erler, T. Ercan, E. Bingol, & S. Orcen (Eds.), i*n Proceedings of the International Symposium on the Geology of the Black Sea Region* (pp. 24–33).

Vialon, P., Ruhland, M., & Grolier, J. (1976). *Eléments de tectonique analytique* (pp. 118). Paris: Masson édit.

Wallace, R. E. (1978). Geometry and rates of change of fault generated range fronts, North-central Nevada. Journal of Research of the U.S. *Geological Survey*, *6*, 637–650.

Wells, S. G., Bullard, T. F., Menges, C. M., Drake, P. G., Karas, P. A., Kelson, K. I., & Wesling, J. R. (1988). Regional variations in tectonic geomorphology along a segmented convergent plate boundary pacific coast of Costa Rica. *Geomorphology*, *1*, 239–265.

Westaway, R. (1994). Present-day kinematics of the Middle East and eastern Mediterranean. *Journal of Geophysical Research*, *99*, 12071–12090.

Wilcox, R. E., Harding, T. P., & Seely, D. R. (1973). Basic wrench tectonics. *AAPG Bulletins*, *57*, 74–96.

Willgoose, G., & Hancock, G. (1998). Revisiting the hypsometric curve as an indicator of form and process in transportlimited catchment. *Earth Surface Processes and Landforms*, *23*, 611–623.

Yıldırım, C. (2014). Relative tectonic activity assessment of the Tuz Gölü fault zone; Central Anatolia, Turkey. *Tectonophysics*, *630*, 183–192.

Yıldırım, C., Melnick, D., Ballato, P., Schildgen, T. F., Echtler, H., Erginal, A. E., … Strecker, M. R. (2013). Differential uplift along the northern margin of the Central Anatolian Plateau: Inferences from marine terraces. *Quaternary. Science Review*, *81*, 12–28.

Yıldırım, C., & Tüysüz, O. (2017). Estimation of the long-term slip, surface uplift and block rotation along the northern strand of the North Anatolian Fault Zone: Inferences from geomorphology of the Almacık Block. *Geomorphology*, *297*, 55–68.

Yılmaz, Y. (2017). Morphotectonic Development of Anatolia and the Surrounding Regions. In I. Çemen & Y. Yılmaz (eds.), *in Active Global Seismology: Neotectonics and Earthquake Potential of the Eastern Mediterranean Region* (pp. 11–91). America: American Geophysical Union, 225.